ACS OMEGA

http://pubs.acs.org/journal/acsodf

Article

Ab Initio Time-Domain Study of Charge Relaxation and Recombination in N-Doped Cu_2O

Jianfeng Su,* Jiao Zhang, Yajie Wang, Changqing Wang, Qiang Niu, Ruirui Sun, and Weiying Zhang

Cite This: *ACS Omega* 2023, 8, 28846−28850

Read Online

ACCESS | Metrics & More | Article Recommendations | Supporting Information

ABSTRACT: Cu_2O is a good photoelectric material with excellent performance, and its crystal structure, electronic structure, and optical properties have been extensively studied. To further illustrate the charge distribution and the carrier transport in this system, the e−h recombination dynamics was studied. It is found that N doping induced a shallower impurity band above the VBM, leading to significant charge localization around the impurity atom. NAMD simulation reveals that the N doping system possesses a longer e−h nonradiative recombination time scale. Therefore, we demonstrate that the formation of the impurity band and charge localization play an essential role in suppressing e−h recombination in N doping systems. This work is conducive for understanding the carrier transport mechanism in N-doped Cu_2O.

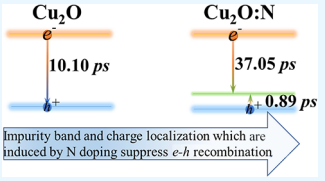

INTRODUCTION

As a p-type semiconductor with an intrinsic direct band gap of 2.17 eV, cuprous oxide (Cu_2O) possesses a set of unique optical and electronic properties.[1,2] In addition, due to its low cost, nontoxicity, and high absorption rate in the visible region, it is regarded as one of the most promising materials for photovoltaic and photocatalytic application.[3−6] According to the Shockley−Queisser limit,[7] Cu_2O has been theoretically predicted to have a maximum power conversion efficiency of approximately 20% for solar cells,[8,9] while the achieved highest efficiency is only about 6.1% by now.[10] Therefore, more research is needed to further optimize the material properties and then to improve the cell efficiency.[11,12] One way which is often used is to modulate the conductivity of the Cu_2O films by doping, and nitrogen has been proved as an effective dopant.[13,14] Several experimental and theoretical studies have been dedicated to study the doping effects of nitrogen on the crystal structure, electronic structure, and optical properties of Cu_2O.[15−17] Researchers found that nitrogen can be easily incorporated into the crystal lattice of Cu_2O at high concentrations to substitute oxygen atoms and act as a p-type dopant, and some reported that an intermediate band forms in the gap by N doping. Nitrogen-doped Cu_2O could act as a possible material for impurity band (IB) solar cells, while the role of the N element in the charge distribution and then carrier transport and lifetimes, which is important in photovoltaic applications, has been of little concern.

In this study, using time-dependent ab initio nonadiabatic molecular dynamics (NAMD) simulations, the electron−hole (e−h) recombination dynamics, which is key to the lifetime of excited carriers in Cu_2O, were presented. The effect of N doping was illustrated. It is found that N doping plays a significant role in modulating the charge distribution except for narrowing the band gap of Cu_2O. NAMD studies further reveal that the N doping sample exhibits smaller NA coupling. Our study demonstrates that the formation of the IB and charge localization play an essential role in suppressing e−h recombination in N doping systems. This work provides an effective way for the design of high-performance solar cells based on Cu_2O.

METHODS

The time-dependent ab initio NAMD simulations are performed using the Hefei-NAMD code.[18] It is convenient to augment the Vienna Ab initio Simulation Package (VASP)[19] with the NAMD capabilities within time-domain density functional theory (DFT).

Geometry optimization, electronic structure calculations, and ab initio molecular dynamics (AIMD) are performed using the VASP. A 2 × 2 × 2 Monkhorst−Pack *k*-point mesh is adopted. The projector augmented wave (PAW)[20] method describes electron−ion interactions. The valence configurations of Cu, O, and N atoms used in the calculations are $3d^{10}$ $4s^1$, $2s^2$ $2p^4$, and $2s^2$ $2p^3$, respectively. In addition, the Perdew−Burke−Ernzerhof (PBE) functional under the generalized gradient approximation (GGA)[21] is applied to treat the exchange-correction interactions. An energy cutoff of 400 eV is used to converge energies and wave functions. To investigate the influence of N dopants on geometry, electronic structure, and charge dynamics, a (3 × 3 × 3) supercell was employed, and two O atoms are uniformly substituted with N, corresponding to 1.2% (atomic fraction) N doping concen-

Received: June 4, 2023
Accepted: July 18, 2023
Published: July 27, 2023

tration. All the structures are fully relaxed until the total energy and the maximum atomic forces are smaller than 10^{-5} eV and 0.01 eV/Å, respectively. Then, the system is heated to 300 K by repeated velocity rescaling. Here, the *K*-point mesh uses a Γ point only because a huge 162-atom supercell is used. After this, a 3 ps AIMD trajectory is obtained using the microcanonical ensemble with a 1 fs time step. The NAMD results are obtained by averaging over 100 random initial configurations selected from the molecular dynamics (MD) trajectory.[22] The e−h nonradiative recombination times were obtained by fitting the charge population using the exponential decay function $f(t) = \exp(-t/\tau) \approx 1 - t/\tau$.[23] This method has been widely used to study photoexcited carrier dynamics in various systems.[24−26] In this calculation, the spin−orbit coupling (SOC) effects on the structural relaxation have not been included to reduce the computational effort because it has been proven that the results of SOC on charge distribution are rather limited.[27]

RESULTS AND DISCUSSION

The supercell model of pure and N-doped Cu_2O considered in the present work is shown in Figure 1. Cu_2O has a high

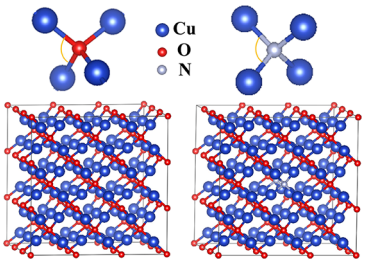

Figure 1. Optimized geometries for pure and N-doped Cu_2O.

symmetry cubic structure (point group: *O4h*; space group: 224, $Pn\bar{3}m$).[28] It has six atoms per unit cell: the oxygen atoms form a bcc lattice, while the copper is on the vertices of a tetrahedron around each oxygen atom. The detailed calculation parameters are displayed in Table S1. The optimized lattice constants are $a = b = c = 4.2696$ Å, which are in good agreement with experimental values.[29] These results implied that our calculation methods are reasonable, and the calculated results should be authentic. In addition, we found that the bond angle of Cu−O−Cu is equal to 109.4712° in pure Cu_2O, while in the N doping model, the bond angle of Cu−N−Cu is 109.5500°, 109.5500°, 108.8184°, 109.5539°, 109.7971°, and 109.5538°, respectively. This indicates that owing to the differences in the ion radius and valence electron configuration between O and N atoms, a lattice distortion occurs. In addition, the evolution of the Cu−O−Cu bond angle and the Cu−N−Cu bond angle along the MD simulation at 300 K is displayed in Figure S1. This indicated that in the N doping system, the lattice distortion is more serious.

The calculated band structure and DOS of pure and N-doped Cu_2O are plotted and compared in Figure 2. As shown in Figure 2a,b, pure Cu_2O is a direct band gap semiconductor with a calculated band gap of 0.54 eV between the VBM and CBM. The PBE-DFT calculation marginally underestimates the band gap relative to experimental results (2.17 eV), while multiple studies have proven that the system underestimate will not affect the ratiocination of the band gap variation tendency.[30] In the case of nitrogen doping, the band gap is

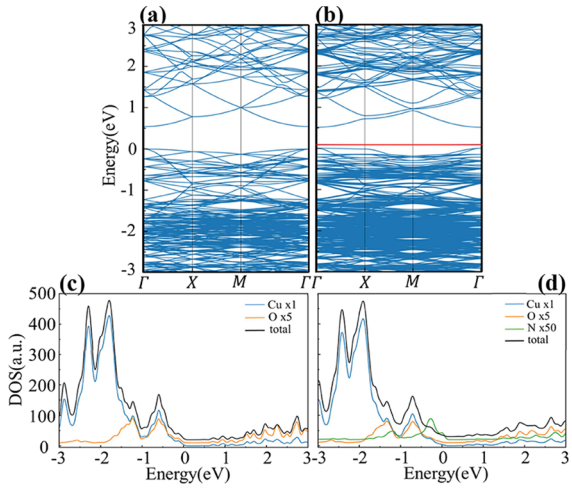

Figure 2. Band structures (a, b) and projected density of states (DOS) (c, d) for pure and N-doped Cu_2O. The Fermi level is set to zero. The impurity energy level was identified by the red line.

narrowed from 0.54 to 0.51 eV slightly. In addition, there is an impurity energy level, which was identified by the red line located above the top of the VBM about 0.09 eV. PDOS plots in Figure 2c,d highlight that the upper valence band is dominated by the Cu-3d states. The lower conduction band exhibits the hybridized states between all atoms. The impurity energy level is mainly derived from the N-2p states, but other electronic states, O-2p and Cu-3p, -3d, and -4s, also contribute to its formation.

To illustrate the effect of lattice distortion, which was induced by N doping on the charge density distribution, the Kohn−Sham orbitals of the CBM and VBM for pure and N-doped Cu_2O are plotted in Figure 3. For the pure system, the

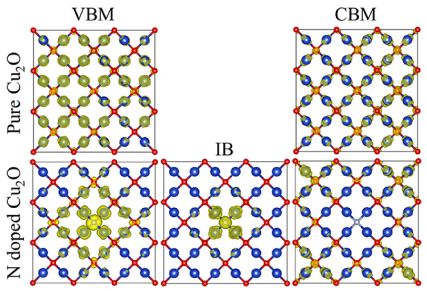

Figure 3. Orbital distribution of the CBM and the VBM for pure and N-doped Cu_2O.

VBM and CBM are distributed on both Cu and O atoms uniformly, which shows a free charge carrier feature. In the N doping system, the VBM was distributed on N atoms and Cu atoms, which were near the N atoms, while the CBM was distributed on Cu and O atoms far away from the doping atoms. The IB was also displayed. The charge is localized around N atoms. Significant charge localization can be observed. According to Ambrosio and Mahata's report, the spatial separation between polaronic holes and electrons were induced by local structural distortions of the sublattice.[27,31] The bond angle variation in doping systems confirmed this phenomenon.

The dynamics of excited charge carriers at a certain temperature can be emulated by regular NAMD simulations. The e−h recombination time is estimated as the time scale

https://doi.org/10.1021/acsomega.3c03916
ACS Omega 2023, 8, 28846−28850

when either the electron or hole reaches the VBM or CBM, respectively. For the systems with the IB in the band gap, it is estimated as the time at which the electron and hole both reach one of the intermediate bands, which are located in the band gap. The results which have been corrected with a scissors operation are shown in Figure 4. The e−h nonradiative

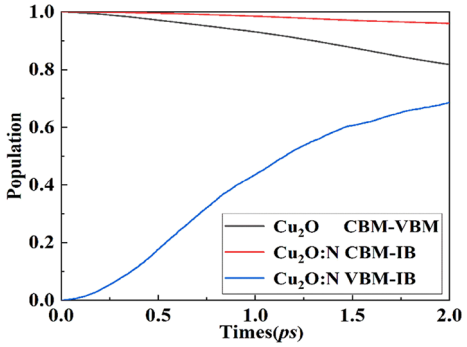

Figure 4. e−h recombination dynamics in pure and N-doped Cu_2O.

recombination times, which were obtained by fitting the charge population using the exponential decay function $f(t) = \exp(-t/\tau) \approx 1 - t/\tau$, are listed in Table 1.[23] The e−h recombination time in the pure system is 10.10 ps. With N doping, the timescale was prolonged to 37.05 ps, which relies on the slower transition between electrons or holes to reach the intermediate band. It is about four times more than the pure system. Zhang et al. also reported that acceptor doping could accelerate charge separation in Cu_2O.[32]

Table 1. Optical Band Gaps, Nonadiabatic Couplings (NACs), and Nonradiative e−h Recombination Time for Pure and N-Doped Cu_2O

	band gap (eV)	NAC (meV)	recombination (ps)
Cu_2O (CBM-VBM)	0.54	3.95	10.10
Cu_2O:N (CBM-IB)	0.51	2.18	37.05
Cu_2O:N (VBM-IB)	0.09	9.78	0.89

In NAMD simulations, the hopping probability of excited e−h between different energy states depends on the NAC elements, which can be written as: $d_{jk} = \langle \varphi_j | \frac{\partial}{\partial t} | \varphi_k \rangle = \frac{\langle \varphi_j | \nabla_R H | \varphi_k \rangle}{\varepsilon_k - \varepsilon_j} \dot{R}$. H is the Kohn−Sham Hamiltonian. φ_j, φ_k, ε_j, and ε_k are the corresponding wave functions and eigenvalues for electronic states j and k. R is the position of the nuclei, and $\dot{R}$ is the velocity of the nuclei.[33] Table 1 shows the averaged NAC results of pure and N-doped Cu_2O at 300 K. In the pure system, the NAC is 3.95 meV. In the N-doped system, the result is 2.18 meV between the CBM and IB and 9.78 meV between the IB and VBM. From the d_{jk} equation, one can see that the NAC elements show strong dependence on the electron−phonon (e−ph) coupling term $\langle \varphi_j | \nabla_R H | \varphi_k \rangle$, energy difference $\varepsilon_k - \varepsilon_j$, and the nuclear velocity $\dot{R}$. Because the nuclear velocity is temperature-dependent, which is comparable in these two systems, we propose that the e−ph coupling and band edge offset are the two crucial factors. The charge density distribution of the CBM and VBM as shown in Figure 3 illustrates that N doping leads to large charge localization. Therefore, even though N doping reduces the band gap slightly, the NAC is still small in this system. The NAC results rationalize the variation tendency of the recombination time scale sufficiently.

To understand the e−ph coupling, we present the fluctuations of the electronic orbital energy difference of related states in Figure 5a, and the corresponding FT spectra

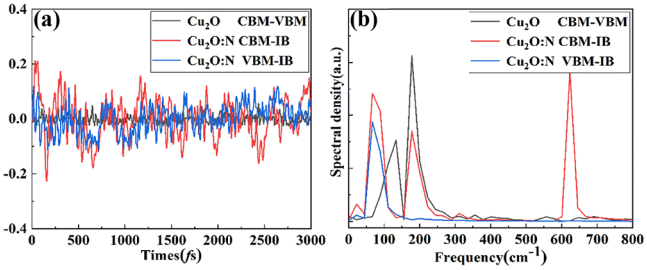

Figure 5. (a) Time evolution of the relevant band gaps at 300 K. (b) Fourier transform (FT) spectra of autocorrelation functions for the fluctuations of the relevant band gap.

are shown in Figure 5b. The fluctuation amplitudes are ∼0.08, 0.2, and 0.4 eV for CBM−VBM of the pure system and CBM-IB and VBM-IB of the N-doped system, respectively. The strength of the electronic-state energy fluctuation amplitude is directly correlated with the strength of e−ph coupling. Furthermore, the FT spectra reveal the dominant phonon modes involved in the NAMD. Figure 5a shows that there is a slightly small energy fluctuation for pure Cu_2O, which is induced by Cu^+ stretching and compression along the face diagonals of the cube (180 cm^{-1}) and the twisting of the tetrahedron of Cu^+(120 cm^{-1}).[34] However, in the N-doped system, a large extent of energy fluctuations indicates that there is a strong e−-ph coupling for the relevant states, which is excited by the rotation of the Cu^+ tetrahedron (88 cm^{-1}), Cu^+ stretching and compression along the face diagonals of the cube (180 cm^{-1}),[34] and stretching vibration of copper(I)−O (622 cm^{-1}).[35] The introduction of N dopants activates more phonon modes due to symmetry breaking.

CONCLUSIONS

In summary, using ab initio NAMD simulations, we have gained deep insight into the nonradiative e−h recombination in the Cu_2O system. Calculation results indicated that N doping induced a shallower IB on the VBM, leading to significant charge localization. Further analysis of orbit distribution combined with the band gap reduction illustrates the variation tendency of NAC, which is the key factor for the hopping probability of excited e−h. Therefore, we demonstrate that the formation of the IB and charge localization play an essential role in suppressing e−h recombination in N doping systems, and it is beneficial to achieve high-efficiency Cu_2O-based optoelectronic devices.

ASSOCIATED CONTENT

Supporting Information

The Supporting Information is available free of charge at https://pubs.acs.org/doi/10.1021/acsomega.3c03916.

Calculation parameters for Cu_2O and Cu_2O:N supercells (3 × 3 × 3); evolution of the Cu−O−Cu bond angle and the Cu−N−Cu bond angle along the AIMD simulation at 300 K; and crystal structure, band structure, and orbital distribution of the CBM and the

https://doi.org/10.1021/acsomega.3c03916
ACS Omega 2023, 8, 28846−28850

VBM for N-doped Cu_2O (N atom was doped not in the neighboring sites) (PDF)

AUTHOR INFORMATION

Corresponding Author

Jianfeng Su − *Department of Mathematics and Physics, Luoyang Institute of Science and Technology, Luoyang 471023, China;* orcid.org/0000-0002-5436-3523; Phone: +86-037965928279; Email: sujianfengvy@163.com

Authors

Jiao Zhang − *Department of Mathematics and Physics, Luoyang Institute of Science and Technology, Luoyang 471023, China*

Yajie Wang − *Department of Mathematics and Physics, Luoyang Institute of Science and Technology, Luoyang 471023, China*

Changqing Wang − *Department of Mathematics and Physics, Luoyang Institute of Science and Technology, Luoyang 471023, China*

Qiang Niu − *Department of Mathematics and Physics, Luoyang Institute of Science and Technology, Luoyang 471023, China*

Ruirui Sun − *Department of Mathematics and Physics, Luoyang Institute of Science and Technology, Luoyang 471023, China*

Weiying Zhang − *School of Physics and Electronic Information, Luoyang Normal University, Luoyang 471022, China*

Complete contact information is available at: https://pubs.acs.org/10.1021/acsomega.3c03916

Notes

The authors declare no competing financial interest.

ACKNOWLEDGMENTS

J.S. acknowledges the support of the Natural Science Foundation of China (Grant No. A050204) and the Natural Science Foundation of Henan province (Grant Nos. 222300420240, 222300420241, 232300420124, and 22A430030). Thanks the team of Professor Jin Zhao in the University of Science and Technology of China.

REFERENCES

(1) Jeong, S. S.; Mittiga, A.; Salza, E.; Masci, A.; Passerini, S. Electrodeposited ZnO/Cu_2O heterojunction solar cells. *Electrochim. Acta* **2008**, *53*, 2226−2231.

(2) Musa, A. O.; Akomolafe, T.; Carter, M. J. Production of cuprous oxide, a solar cell material, by thermal oxidation and a study of its physical and electrical properties. *Sol. Energy Mater. Sol. Cells* **1998**, *51*, 305−316.

(3) Sekkat, A.; Nguyen, B. V. H.; Masse De La Huerta, C. A.; Rapenne, L.; Bellet, D.; Kaminski Cachopo, A.; Chichignoud, G.; Muñoz Rojas, D. Open-air printing of Cu_2O thin films with high hole mobility for semitransparent solar harvesters. *Commun. Mater.* **2021**, *2*, 78.

(4) Zang, Z. G. Efficiency enhancement of ZnO/Cu_2O solar cells with well oriented and micrometer grain sized Cu_2O films. *Appl. Phys. Lett.* **2018**, *112*, No. 042106.

(5) Bendavid, L. I.; Carter, E. A. First-principles predictions of the structure, stability, and photocatalytic potential of Cu_2O surfaces. *J. Phys. Chem. B* **2013**, *117*, 15750−15760.

(6) Qin, C.; Chen, X. H.; Liang, R.; Jiang, N.; Zheng, Z. C.; Ye, Z. Z.; Zhu, L. P. Fabricating high-quality Cu_2O photocathode by magnetron sputtering: insight into defect states and charge carrier collection in Cu_2O. *ACS Appl. Energy Mater.* **2022**, *5*, 14410−14422.

(7) Shockley, W.; Queisser, H. J. Detailed balance limit of efficiency of PN junction solar cells. *J. Appl. Phys.* **1961**, *32*, 510−519.

(8) Meyer, B. K.; Polity, A.; Reppin, D.; Becker, M.; Hering, P.; Kramm, B.; Klar, P. J.; Sander, T.; Reindl, C.; Heiliger, C.; et al. Chapter six-the physics of copper oxide (Cu_2O). *Semicond. Semimet.* **2013**, *88*, 201−226.

(9) Olsen, L. C.; Addis, F. W.; Miller, W. Experimental and theoretical studies of Cu_2O solar cells. *Sol. Cells* **1982**, *7*, 247−279.

(10) Minami, T.; Nishi, Y.; Miyata, T. H. Heterojunction solar cell with 6% efficiency based on an n-type aluminum-gallium-oxide thin film and p-type sodium-doped Cu_2O sheet. *Appl. Phys. Express* **2015**, *8*, No. 022301.

(11) Jo, J.; Deng, Z.; Sanders, N.; Kioupakis, E.; Peterson, R. L. Experimental and theoretical study of hole scattering in RF sputtered p-type Cu_2O thin films. *Appl. Phys. Lett.* **2022**, *120*, No. 112105.

(12) Sekkat, G.; Liedke, M. O.; Nguyen, V. H.; Butterling, M.; Baiutti, F.; de Dios Sirvent Veru, J.; Weber, M.; Rapenne, L.; Bellet, D.; Chichignoud, G.; et al. Chemical deposition of Cu_2O films with ultra-low resistivity: correlation with the defect landscape. *Nat. Commun.* **2022**, *13*, 5322.

(13) Zhao, Z.; He, X.; Yi, J.; Ma, C.; Cao, Y.; Qiu, J. First-principles study on the doping effects of nitrogen on the electronic structure and optical properties of Cu_2O. *RSC Adv.* **2013**, *3*, 84.

(14) Li, J. Q.; Mei, Z. X.; Liu, L. S.; Liang, H. L.; Azarov, A.; Kuznetsov, A.; Liu, Y. P.; Ji, A. L.; Meng, Q. B.; Du, X. L. Probing defects in nitrogen-doped Cu_2O. *Sci. Rep.* **2014**, *4*, 7240.

(15) Wang, Y.; Ghanbaja, J.; Horwat, D.; Yu, L.; Pierson, J. F. Nitrogen chemical state in N-doped Cu_2O thin films. *Appl. Phys. Lett.* **2017**, *110*, No. 131902.

(16) Benz, J.; Hering, K. P.; Kramm, B.; Polity, A.; Klar, P. J.; Siah, S. C.; Buonassisi, T. The influence of nitrogen doping on the electrical and vibrational properties of Cu_2O. *Phys. Status Solidi B* **2017**, *254*, No. 1600421.

(17) T-Thienprasert, J.; Limpijumnong, S. Identification of nitrogen acceptor in Cu_2O: First-principles study. *Appl. Phys. Lett.* **2015**, *107*, No. 221905.

(18) Zheng, Q. J.; Chu, W. B.; Zhao, C. Y.; Zhang, L. L.; Guo, H. L.; Wang, Y. N.; Jiang, X.; Zhao, J. Ab initio nonadiabatic molecular dynamics investigations on the excited carriers in condensed matter systems. *WIREs Comput. Mol. Sci.* **2019**, *9*, No. e1411.

(19) Kresse, G.; Furthmüller, J. Efficient iterative schemes forab initiototal-energy calculations using a plane-wave basis set. *Phys. Rev. B* **1996**, *54*, 11169−11186.

(20) Blochl, P. E. Projector augmented-wave method. *Phys. Rev. B* **1994**, *50*, 17953−17979.

(21) Perdew, J. P.; Burke, K.; Ernzerhof, M. Generalized gradient approximation made simple. *Phys. Rev. Lett.* **1996**, *77*, 3865−3868.

(22) Tully, J. C. *Classical and quantum dynamics in condensed phase simulations*; World Scientific Press: Singapore, 1998.

(23) Li, W.; Tang, J. F.; Casanova, D.; Prezhdo, O. V. Time-Domain ab Initio Analysis Rationalizes the Unusual Temperature Dependence of Charge Carrier Relaxation in Lead Halide Perovskite. *ACS Energy Lett.* **2018**, *3*, 2713−2720.

(24) Zhang, L. L.; Chu, W. B.; Zheng, Q. J.; Zhao, J. Effects of oxygen vacancies on the photoexcited carrier lifetime in rutile TiO_2. *Phys. Chem. Chem. Phys.* **2022**, *24*, 4743−4750.

(25) Shi, Y. L.; Muztoba, R.; Álvaro, V.; Zhao, J.; Wissam, A. S. Controlling the Nucleation and Growth of Ultrasmall Metal Nanoclusters with MoS_2 Grain Boundaries. *Nanoscale* **2022**, *14*, 617−625.

(26) Chu, W. B.; Tan, S. J.; Zheng, Q. J.; Fang, W.; Feng, Y. X.; Prezhdo, O. V.; Wang, B.; Li, X. Z.; Zhao, J. Ultrafast charge transfer coupled to quantum proton motion at molecule/metal oxide interface. *Sci. Adv.* **2022**, *8*, No. eabo2675.

(27) Mahata, A.; Meggiolaro, D.; Angelis, F. D. From Large to Small Polarons in Lead, Tin and Mixed Lead-Tin Halide Perovskites. *J. Phys. Chem. Lett.* **2019**, *10*, 1790−1798.
(28) Ruiz, E.; Alvarez, S.; Alemany, P.; Evarestov, R. A. Electronic structure and properties of Cu_2O. *Phys. Rev. B* **1997**, *56*, 7189.
(29) Werner, A.; Hocheimer, H. D. High-pressure x-ray study of Cu_2O and Ag_2O. *Phys. Rev. B* **1982**, *25*, 5929.
(30) Isseroff, L. Y.; Carter, E. A. Importance of reference Hamiltonians containing exact exchange for accurate one-shot GW calculations of Cu_2O. *Phys. Rev. B* **2012**, *85*, No. 235142.
(31) Meggiolaro, D.; Ambrosio, F.; Mosconi, E.; Mahata, A.; Angelis, F. D. Polarons in Metal Halide Perovskites. *Adv. Energy Mater.* **2020**, *10*, No. 1902748.
(32) Zhang, M. M.; Wang, J. J.; Xue, H.; Zhang, J. F.; Peng, S. J.; Han, X. P.; Deng, Y. D.; Hu, W. B. Acceptor-doping accelerated charge separation in Cu_2O photocathode for photoelectrochemical water splitting: a theoretical and experimental study. *Angew. Chem., Int. Ed.* **2020**, *59*, 18463−18467.
(33) Reeves, K. G.; Schleife, A.; Correa, A. A.; Kanai, Y. Role of Surface Termination on Hot Electron Relaxation in Silicon Quantum Dots: A First-Principles Dynamics Simulation Study. *Nano Lett.* **2015**, *15*, 6429−6433.
(34) Carabato, C. Lattice Vibrations of Cu_2O at the Long Wave Limit. *Phys. Status Solidi B* **1970**, *37*, 773−779.
(35) Kumar, N.; Parui, S. S.; Limbu, S.; Mahato, D. K.; Tiwari, N.; Chauhan, R. N. Structural and optical properties of sol-gel derived CuO and Cu_2O nanoparticles. *Mater. Today: Proc.* **2021**, *41*, 237−241.

https://doi.org/10.1021/acsomega.3c03916
ACS Omega 2023, 8, 28846−28850